Journal of Agricultural Engineering

eISSN: 2239-6268 https://www.agroengineering.org/

Design of attitude-adjustable chassis and dynamic stress analysis of key components for crawler combine harvester

Jinpeng Hu,[1] Yang Yu,[1,2,3] Tianle Ma,[1] Peng Liu,[1] Lizhang Xu[1,2,3]

[1]College of Agricultural Engineering, Jiangsu University, Zhenjiang
[2]Key Laboratory for Theory and Technology of Intelligent Agricultural Machinery and Equipment of Jiangsu University, Zhenjiang
[3]Jiangsu Province and Education Ministry Co-sponsored Synergistic Innovation Center of Modern Agricultural Equipment, Zhenjiang, China

Corresponding author: Yang Yu, College of Agricultural Engineering, Jiangsu University, Zhenjiang, 212013, China. E-mail: yu_yang@ujs.edu.cn

Key words: crawler combine harvester; attitude adjusting mechanism; rigid flexible coupling; dynamic stress.

Table S1. Analysis of variance of response surface test results.

Key components	Source of variance	Total variance	Degree of freedom	Mean square deviation	*F* value	*p-value*	Significance
Left front rotational arm	Model	52923.22	9	5880.358	155.9032	< 0.0001	**
	A	8624.769	1	8624.769	228.6646	< 0.0001	**
	B	1111.491	1	1111.491	29.46844	0.001	**
	C	38834.62	1	38834.62	1029.604	< 0.0001	**
	AB	353.8161	1	353.8161	9.380564	0.018252	*
	AC	44.09624	1	44.09624	1.169103	0.315422	
	BC	258.679	1	258.679	6.858237	0.034468	*
	A^2	148.2476	1	148.2476	3.93042	0.087854	
	B^2	1724.67	1	1724.67	45.72537	0.000262	**
	C^2	2003.389	1	2003.389	53.11492	0.000164	**
	Residual	264.026	7	37.718			
	Lack of fit	162.4127	3	54.13758	2.131122	0.239022	
	Pure error	101.6133	4	25.40332			
	Sum	53187.25	16				
Left rear rotational arm	Model	41449.46585	9	4605.496	472.0906	< 0.0001	**
	A	4211.554753	1	4211.555	431.7092	< 0.0001	**
	B	4534.852613	1	4534.853	464.8492	< 0.0001	**
	C	3982.111903	1	3982.112	408.19	< 0.0001	**
	AB	23.3289	1	23.3289	2.39135	0.165929	
	AC	398.9007563	1	398.9008	40.88968	0.000369	**
	BC	1124.9316	1	1124.932	115.3121	< 0.0001	**
	A^2	19156.297	1	19156.3	1963.634	< 0.0001	**
	B^2	2.135250592	1	2.135251	0.218876	0.654114	
	C^2	6573.923385	1	6573.923	673.866	< 0.0001	**
	Residual	68.28874875	7	9.755536			
	Lack of fit	20.10076875	3	6.700256	0.556177	0.671269	
	Pure error	48.18798	4	12.047			
	Sum	41517.7546	16				

*Significant; **very significant.

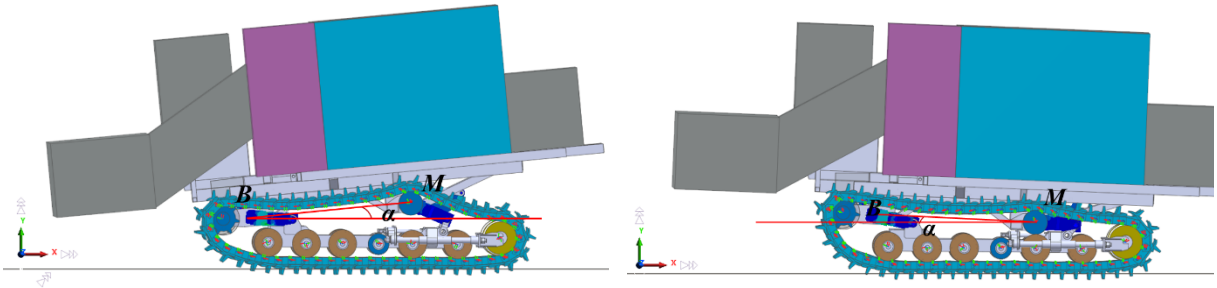

(a) Forward tilting process of chassis (b) Backward tilting process of chassis

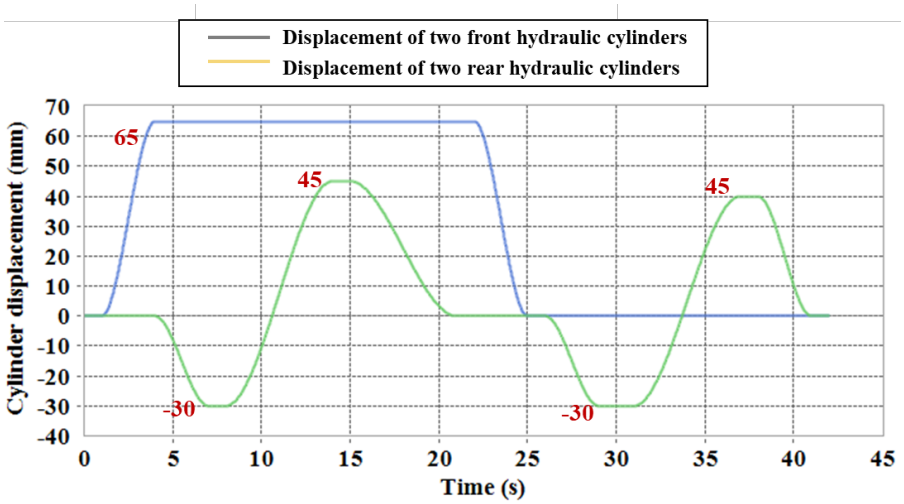

(c) Displacement changes of the front and rear cylinders

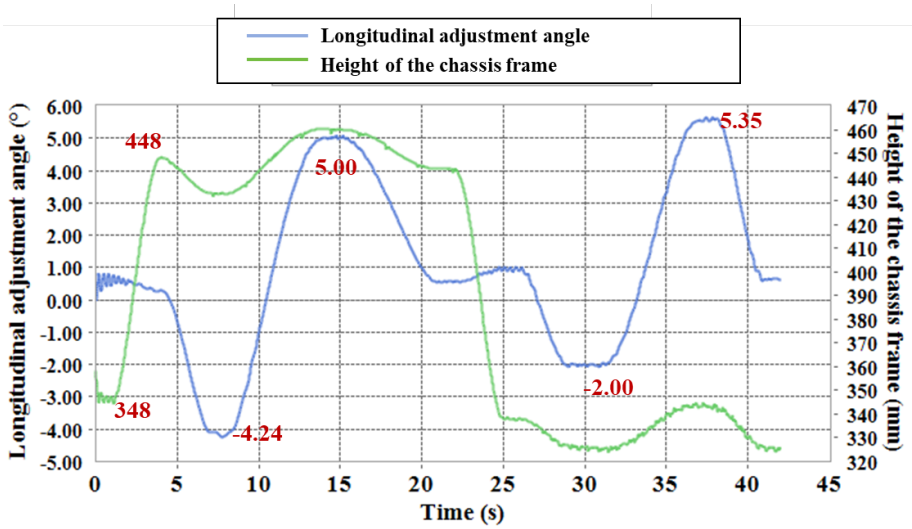

(d) Longitudinal angle changes of the crawler harvester.

Figure S1. Simulation results of longitudinal adjustment.

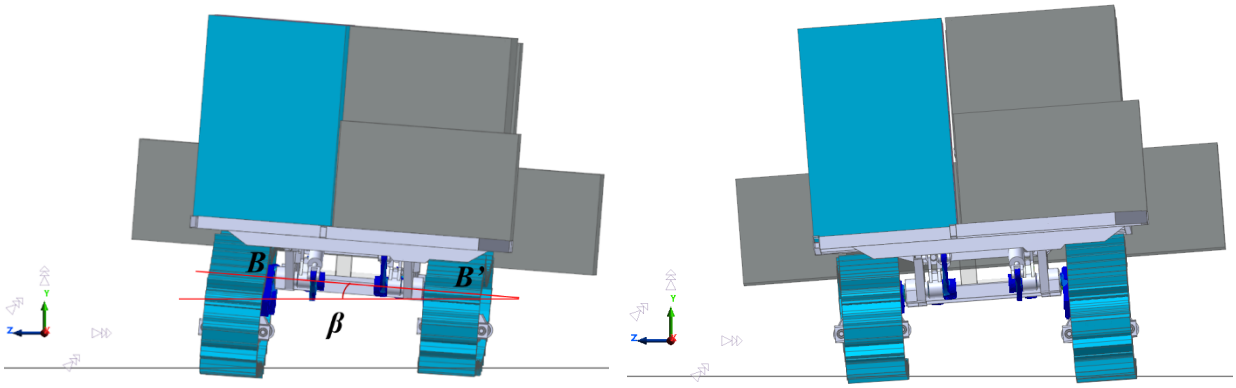

(a) Right tilting process of chassis

(b) Left tilting process of chassis

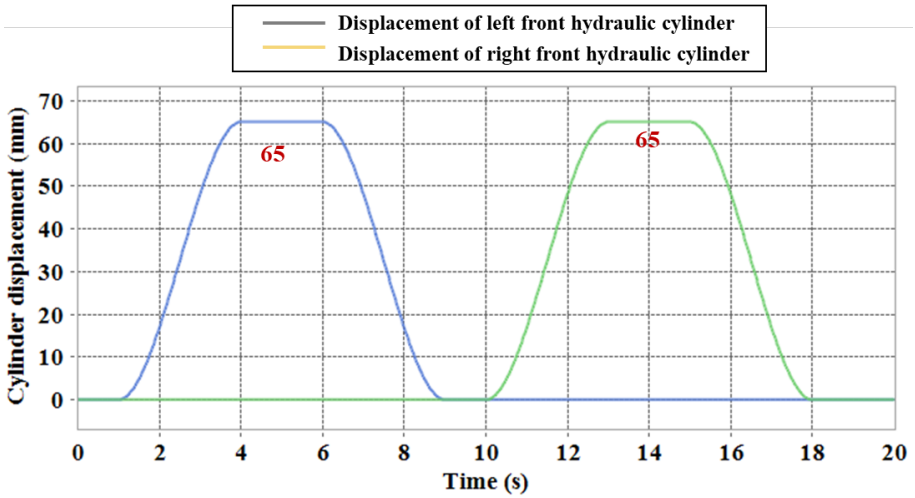

(c) Displacement changes of the front cylinders

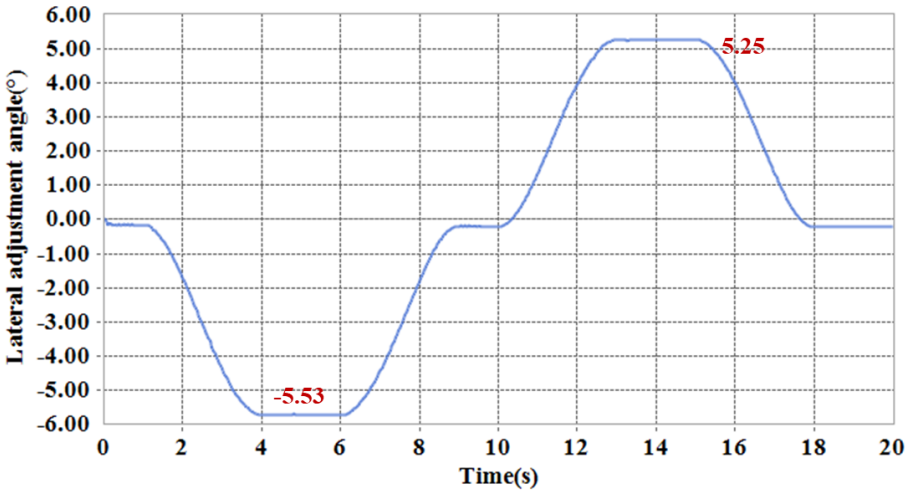

(d) Lateral angle changes of the crawler harvester

Figure S2. Simulation results of lateral adjustment.

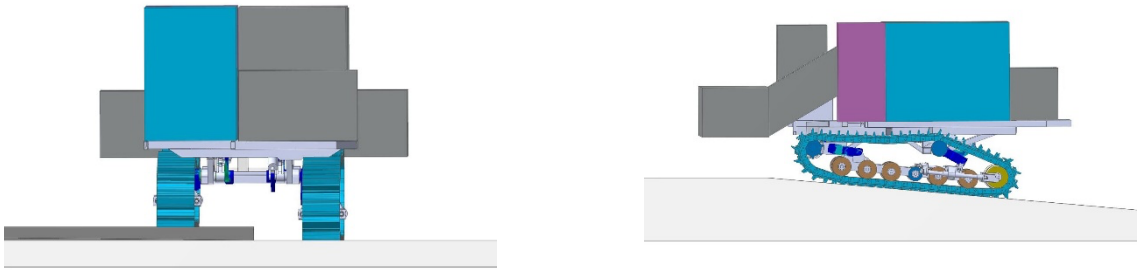

(a) Lateral adjustment simulation (b) Longitudinal adjustment simulation

Figure S3. Rigid-flexible coupling simulation of attitude adjustable chassis.

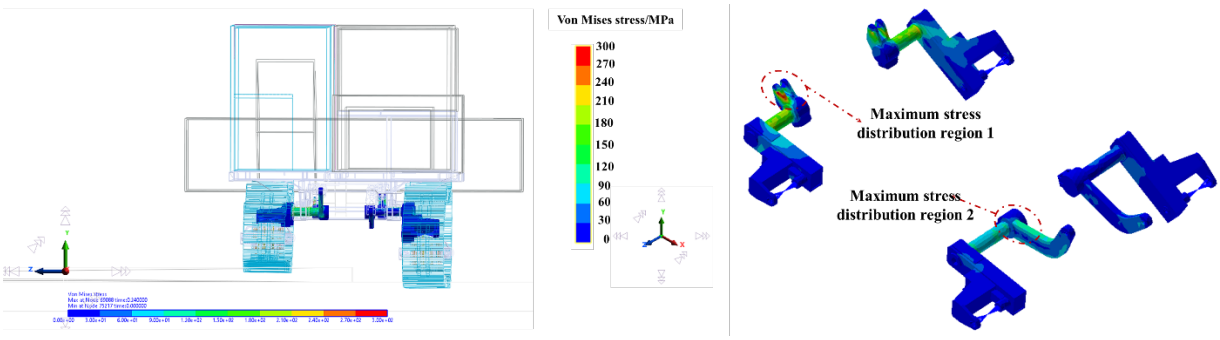

(a) Stress distribution of the rotational arms under the maximum left tilt leveling condition

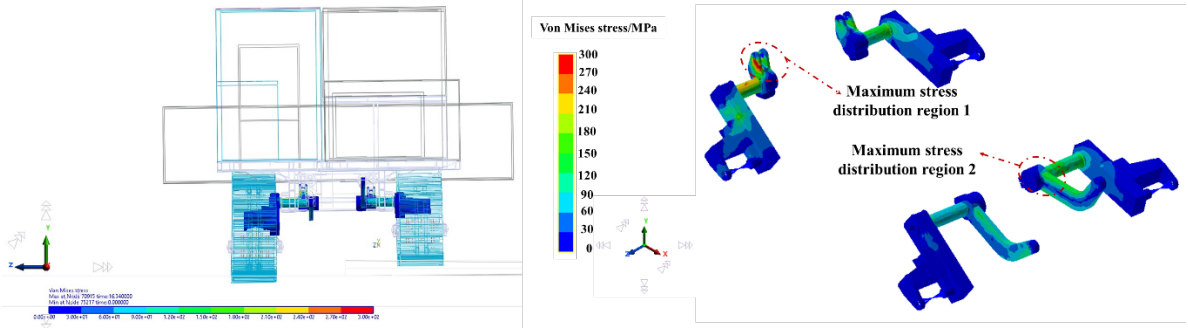

(b) Stress distribution of the rotational arms under the maximum right tilt leveling condition

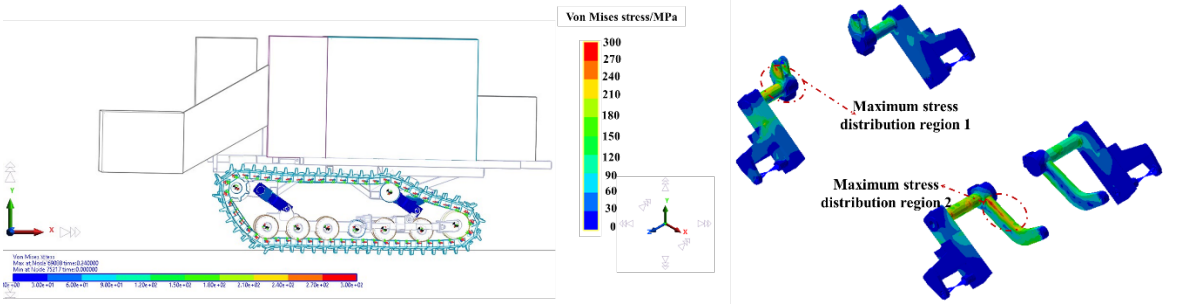

(c) Stress distribution of the rotational arms under the maximum lifting condition

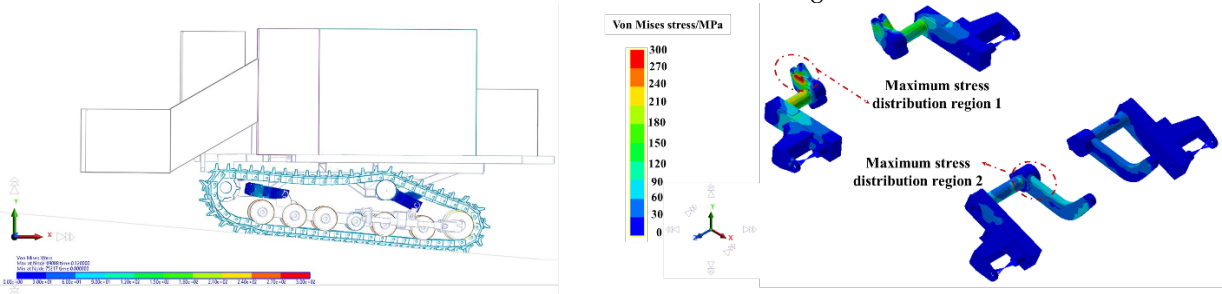

(d) Stress distribution of the rotational arms under the maximum forward leveling condition

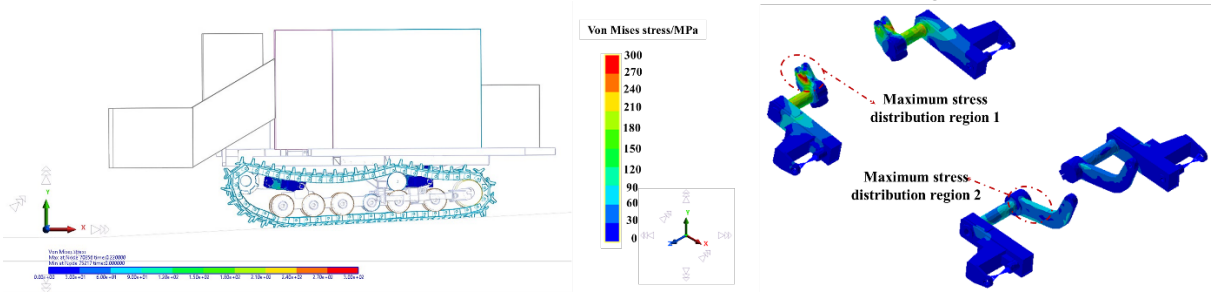

(e) Stress distribution of the rotational arms under the maximum backward tilt leveling condition

Figure S4. Dynamic stress cloud diagram of key components under typical working conditions.

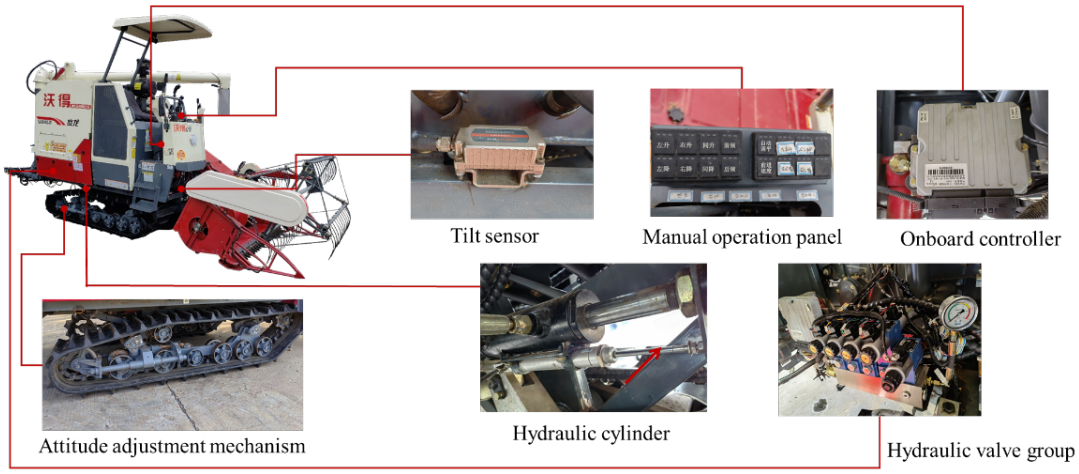

Figure S5. System integration of attitude adjustment chassis prototype.

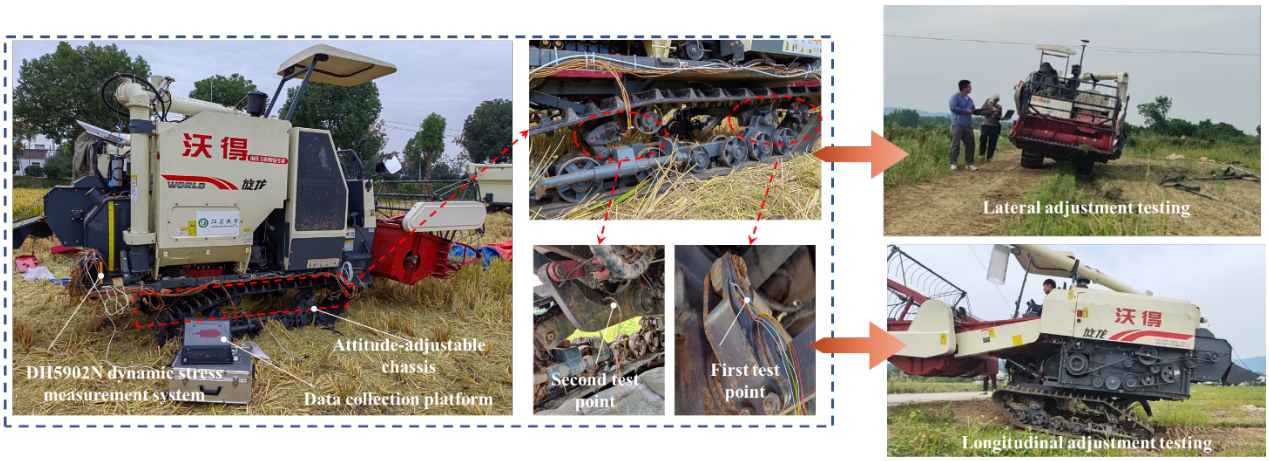

Figure S6. Dynamic stress test site of attitude adjustment mechanism.

(a) Actual lateral adjustment scenario in the field

(b) Actual longitudinal adjustment scenario in the field

Figure S7. Cylinder displacement and adjustment angle data measuring on-site.

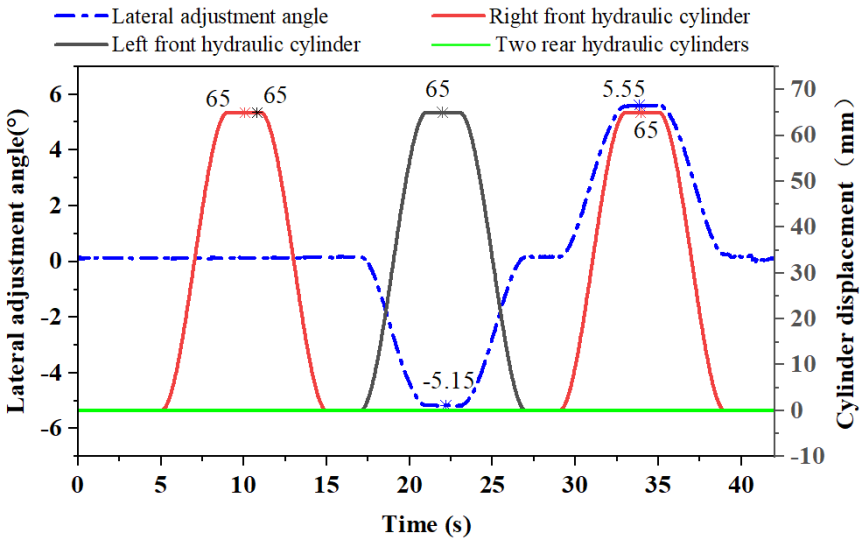

Figure S8. Measured data of lateral adjustment angle, overall lifting height, and cylinder displacement.

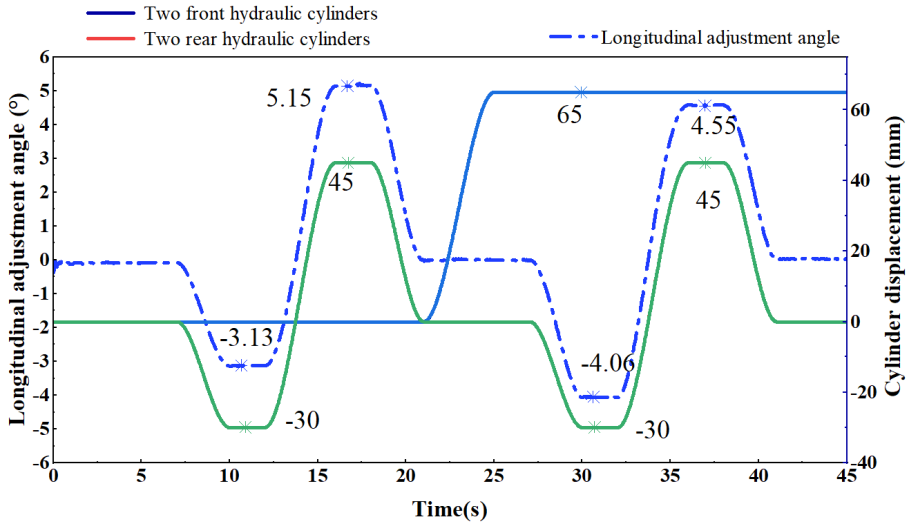

Figure S9. Measured data of longitudinal adjustment angle and cylinder displacement.

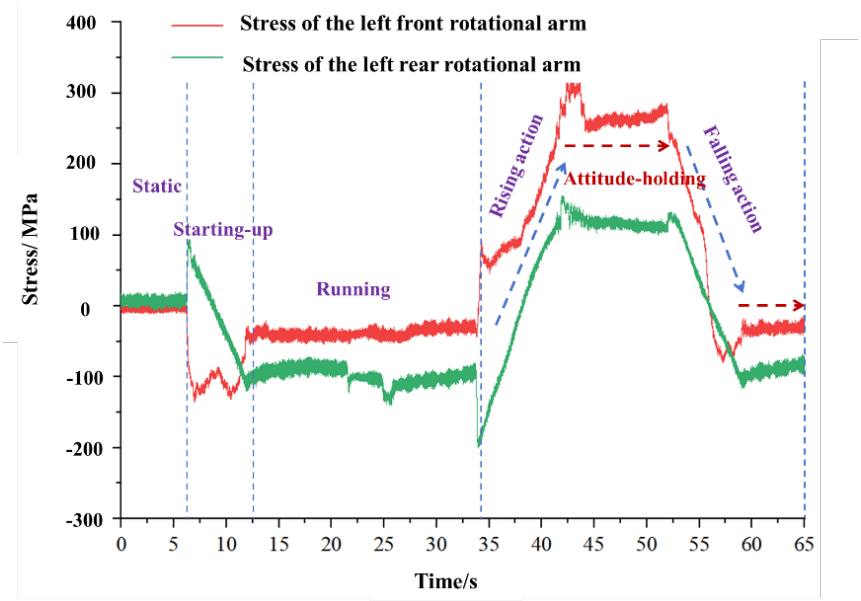

Figure S10. Dynamic stress curve of the left front and rear rotational arms during the lifting of the chassis.

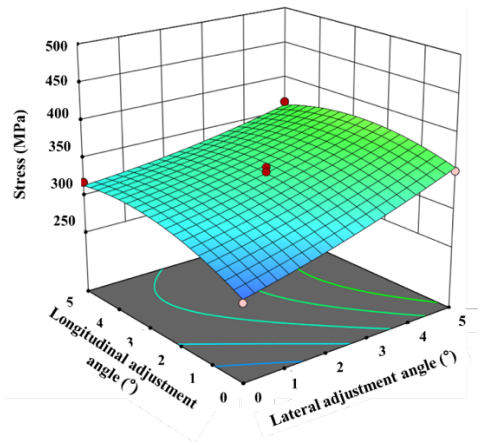

(a) Interaction between longitudinal and lateral adjustment angle

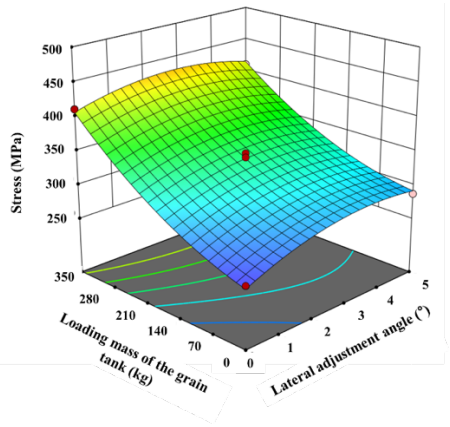

(b) Interaction between loading mass of the grain tank and lateral adjustment angle

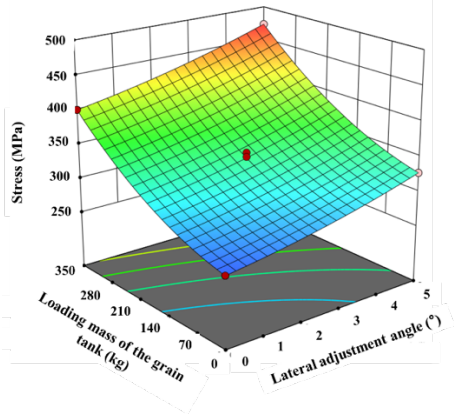

(c) Interaction between lateral adjustment angle and loading mass of the grain tank

Figure S11. The interaction of various factors on the stress of the left front rotational arm.

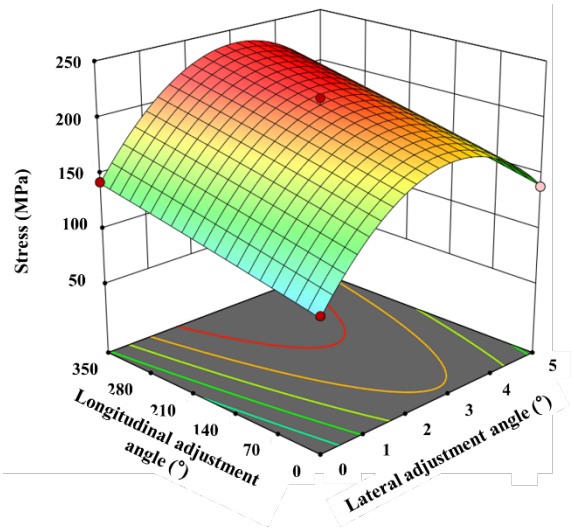

(a) Interaction between longitudinal and lateral adjustment angle

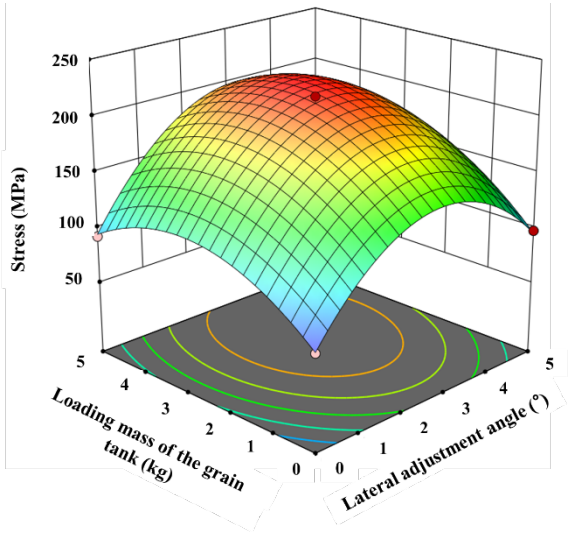

(b) Interaction between lateral adjustment angle and loading mass of the grain tank

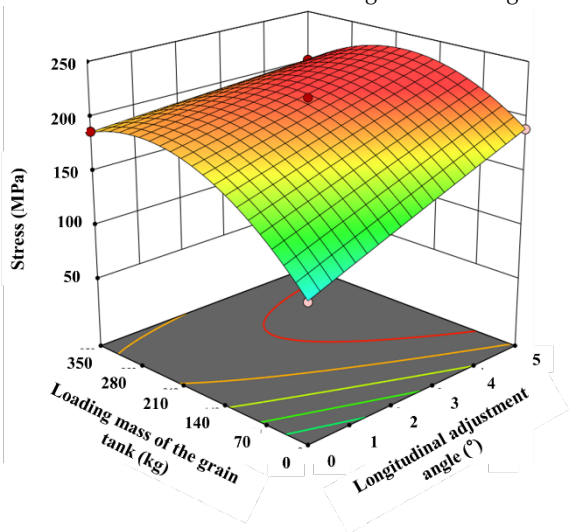

(c) Interaction between longitudinal adjustment angle and loading mass of the grain tank

Figure S12. The interaction of various factors on the stress of the left rear rotational arm.